Fuel 399 (2025) 135685

Contents lists available at ScienceDirect

Fuel

journal homepage: www.elsevier.com/locate/fuel

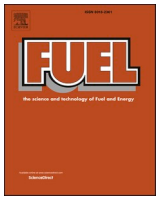

Full Length Article

Chemical looping oxygen uncoupling of biochar using CuO: Influence of oxygen carrier on combustion efficiency☆

Fatih Güleç [a,b,*], Ciaran Moyles [a], Harrison Tagg [a], Alexander Marshall [a], Jack Craft [a], Andrew Batchelor [c], Gabriela Duran-Jimenez [a,c]

[a] Department of Chemical and Environmental Engineering, University of Nottingham, Nottingham NG7 2RD, UK
[b] Low Carbon Energy and Resources Technologies Research Group, Faculty of Engineering, University of Nottingham, Nottingham NG7 2TU, UK
[c] Advanced Materials Research Group, Faculty of Engineering, University of Nottingham, Nottingham NG7 2RD, UK

ARTICLE INFO

Keywords:
Biochar
Chemical looping combustion
Advanced combustion
Cu-based oxygen carrier
CO_2-negative
BECCS

ABSTRACT

Despite the consensus on the urgent need to mitigate climate change by reducing CO2 emissions, technological advancements lag the escalating levels of CO_2. This study investigates the impact of process conditions and oxygen carrier quality on the chemical looping oxygen uncoupling (CLOU) of biochar with CuO as a promising bioenergy production with CO_2 capture and storage (BECCS) approach. This work offers new insights into the role of CuO synthesis method and material source on biochar combustion efficiency in a CLOU framework, comparing both commercial and in-house formulations. Combustion efficiency increases from 67.9 vol% at 750 °C to 98.2 vol% at 900 °C. The stoichiometric ratio also influenced performance, improving from 71.2 vol% at a ratio of 1.0 to 95.7 vol% at 1.5. Higher-quality CuO samples, such as CuO (Honeywell), demonstrated superior performance, achieving 98.3 vol% efficiency compared to 71.2 vol% for CuO (Inoxia) at 850 °C. CuO (Honeywell) also exhibited greater stability across multiple redox cycles, maintaining 99.0 vol% capacity after six cycles, while CuO (Inoxia) suffered a significant decline to 84 vol% due to sintering and agglomeration. Lab-prepared Cu80Al20-WI displayed stable performance, retaining 97.1 vol% after six cycles, outperforming Cu80Al20-CP, which degraded to 83.9 vol%. This performance was mainly attributed to gas diffusional effect and larger availability of active sites in Cu80Al20-WI for oxygen in reduction/oxidation CLC processes. These results highlight the importance of optimising both process conditions and oxygen carrier quality for efficient CLOU applciaiton.

1. Introduction

The growing challenge of global CO_2 emissions has reached critical levels, as highlighted at COP27 in 2022 [1], where it was reported that current emissions put the world on track for over 2 °C of warming, well beyond the COP26 goal of limiting warming to 1.5 °C and achieving net-zero emissions by mid-century [2]. Global energy-related CO_2 emissions increased by 0.9 % in 2022, reaching a record high of 36.8 billion metric tonnes [3]. The gap between current trajectories and the 1.5 °C target is projected to be 19–23 $GtCO_2$eq by 2030, which is about 50 % of current global emissions [4]. Similar to the global target [5] the UK's Net Zero Strategy is aligned with the global aim to remove between 75 and 81 $MtCO_2$/yr by 2050.

Among different technologies, carbon capture and storage (CCS) technologies have been shown to be effective in reducing CO_2 emissions; however, they have several limitations. This technology often relies on energy-intensive CO_2 separation and storage processes, making it costly and inefficient for large-scale applications [6]. Therefore, developing carbon–neutral and carbon-negative technologies that include more economically viable CO_2 separation methods is crucial to reduce dependence on conventional CCS [7]. Carbon-negative technologies, such as Bioenergy with Carbon Capture and Storage (BECCS), are becoming increasingly important [1,8,9] as by combining biomass, a renewable resource [10] that is carbon–neutral at the point of combustion with CCS, BECCS offers a pathway to achieving net-negative CO_2 emissions [11]. This is especially vital given that biomass combustion, which contributed 11 % of the UK's electricity in 2022 [8], must evolve from a carbon–neutral to a carbon-negative solution to have a more

☆ This article is part of a special issue entitled: 'CCL-2025' published in Fuel.

* Corresponding author.
E-mail addresses: Fatih.Gulec1@nottingham.ac.uk, gulec.fatih@outlook.com (F. Güleç).

https://doi.org/10.1016/j.fuel.2025.135685
Received 17 December 2024; Received in revised form 9 May 2025; Accepted 13 May 2025
Available online 16 May 2025

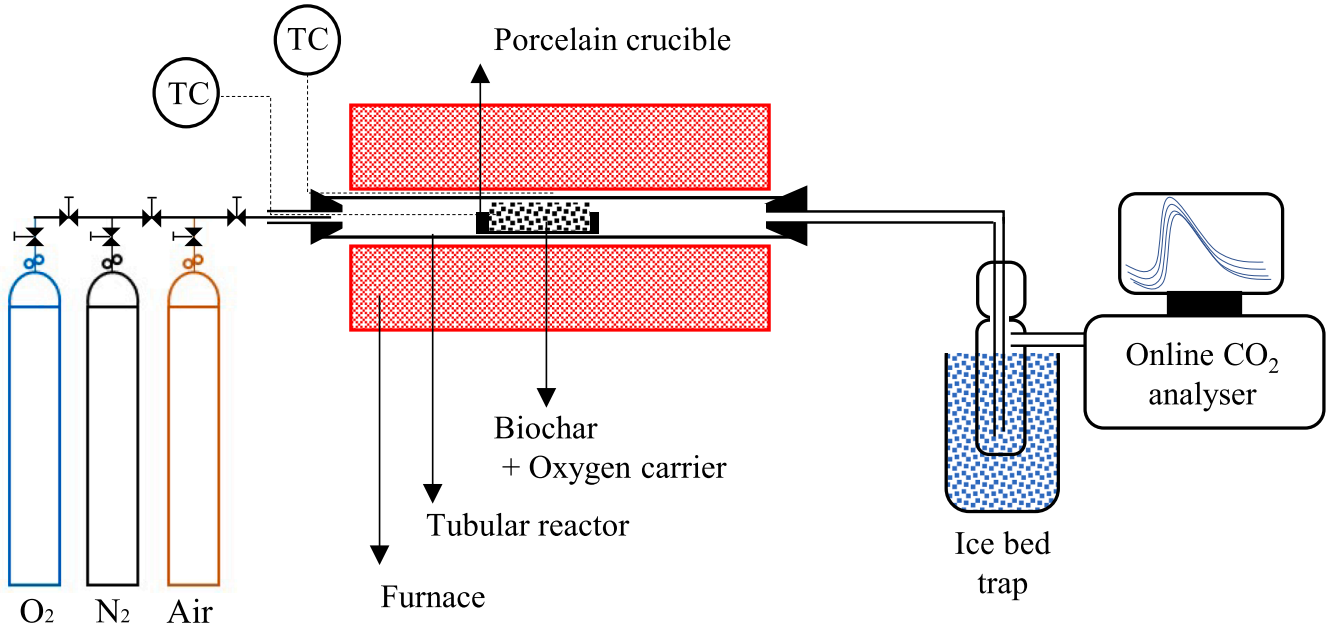

Fig. 1. Chemical looping combustion and oxygen uncoupling experimental set-up.

Table 1
Ultimate and Proximate analysis, of whitewood and biochar produced at 650 °C.

Feedstocks	Unit	Whitewood	*WW-Biochar*
Ultimate analysis (daf) [a]			
Carbon (C)	(wt.%)	46.5 ± 0.10	90.0 ± 0.08
Hydrogen (H)	(wt.%)	6.6 ± 0.09	2.3 ± 0.02
Nitrogen (N)	(wt.%)	2.6 ± 0.03	0.7 ± 0.01
Oxygen[b] (O)	(wt.%)	44.3 ± 0.02	7.0 ± 0.08
Proximate analysis[c]			
Moisture content (M)	(wt.%)	6.60 ± 0.10	5.80 ± 0.67
Volatile matter (VM)	(wt.%)	80.6 ± 1.82	11.0 ± 0.07
Fixed carbon (FC)	(wt.%)	12.4 ± 1.73	82.1 ± 1.03
Ash (A)	(wt.%)	0.40 ± 0.01	1.10 ± 0.29

[a] Dry Ash Free Basis (daf).
[b] Oxygen content was determined by difference.
[c] As received.

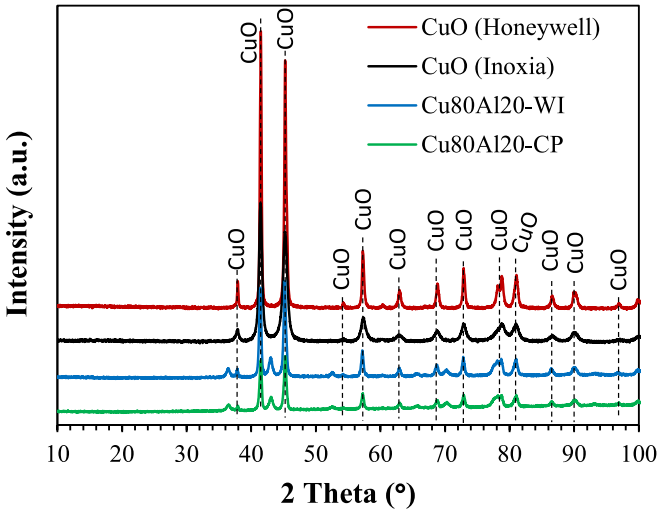

Fig. 2. XRD results of four CuO samples: commercially supplied; CuO (Honeywell) and CuO (Inoxia), and synthesised; Cu80Al20-CP and Cu80Al20-WI.

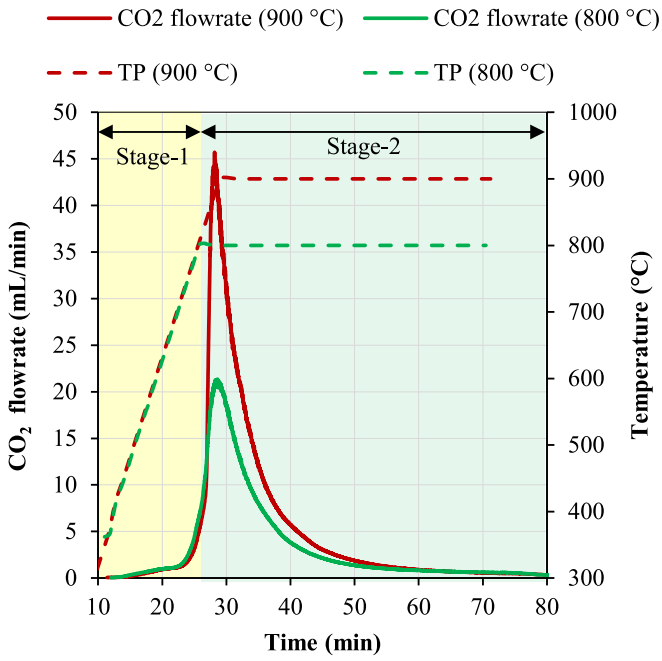

Fig. 3. Combustion profile of biochar with CuO (Inoxia) at 800 °C and 900 °C.

Table 2
Effect of temperature on combustion efficiency of biochar with CuO (ϕ = 1.0).

Temperature (°C)	$V_{CO2,max}$ (mL)	$V_{CO2,measured}$ (mL)	Combustion Efficiency (vol.%)
900	336.1	306.9	98.2 ± 2.4
850	336.1	239.3	71.2 ± 2.7
800	336.1	228.2	67.9 ± 4.3
750	336.1	195.1	58.0 ± 4.0

substantial impact on climate change by the Department for Energy Security and Net Zero, 2023.

Chemical Looping Combustion (CLC) stands out as revolutionary

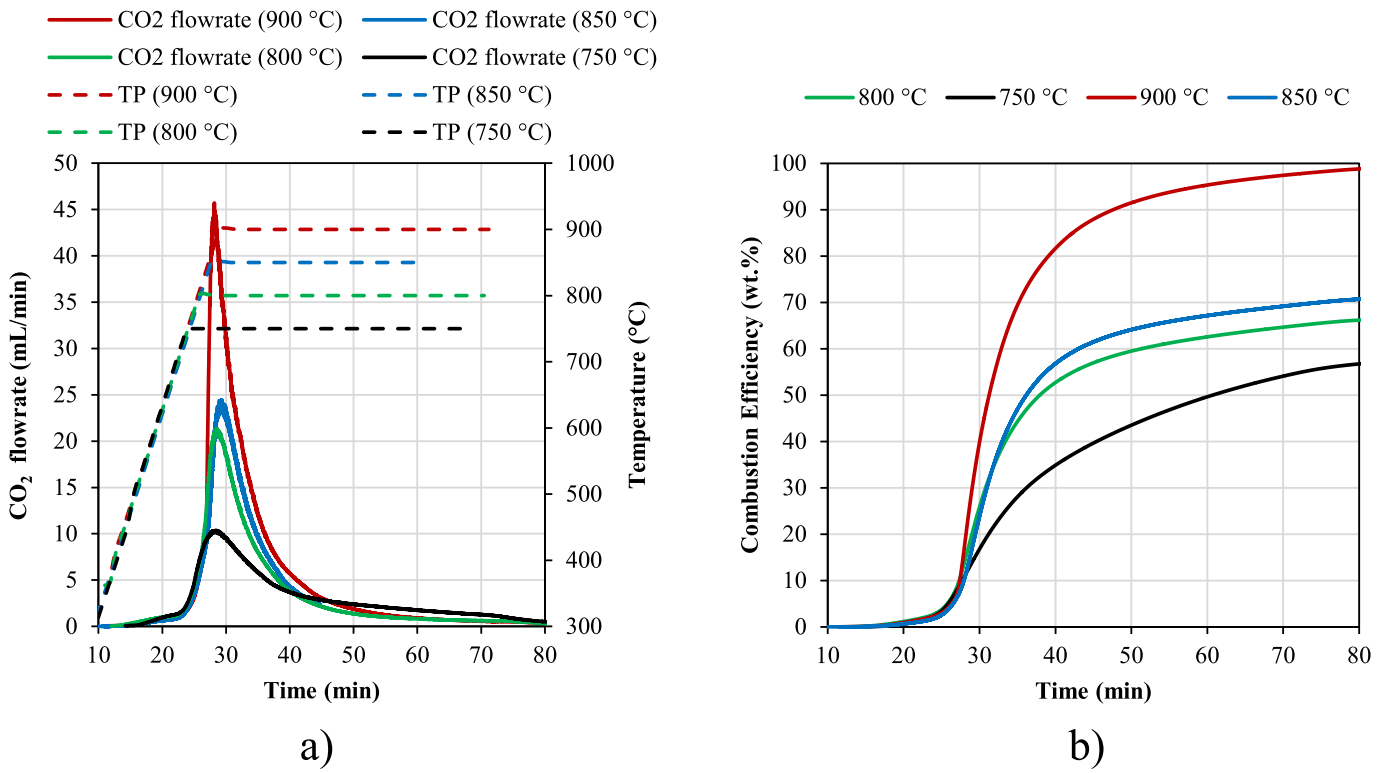

Fig. 4. A) co_2 flowrate and b) Combustion efficiency of the biochar combustion with CuO (Inoxia) at 750–900 °C.

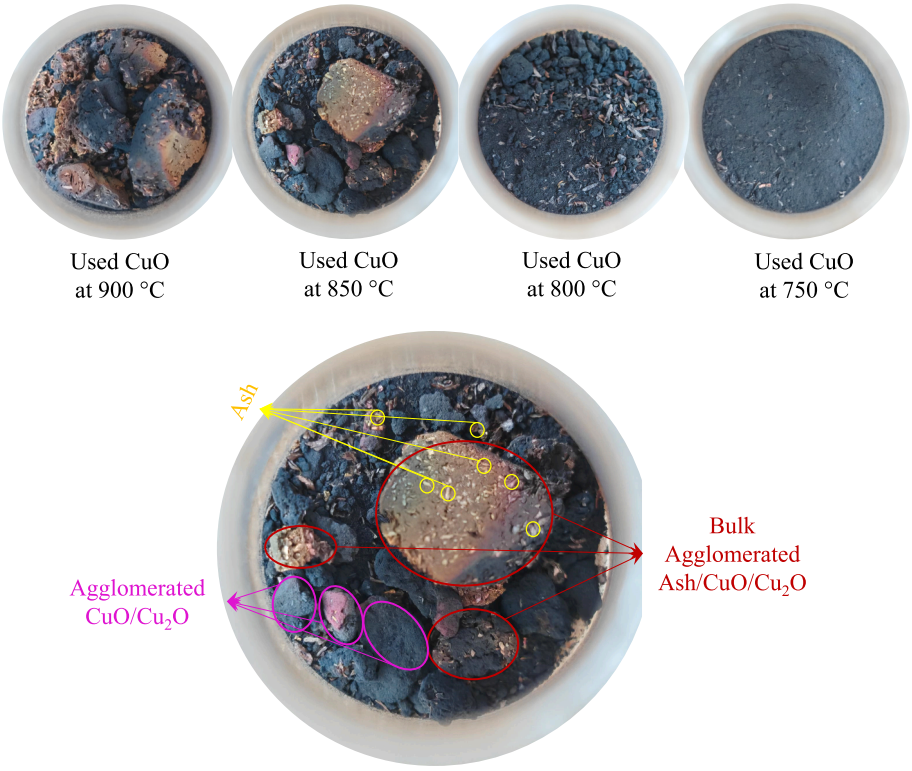

Fig. 5. Visual images of used CuO (Inoxia) in the combustion of biochar at 750–900 °C.

technology and presents a particularly promising approach [12]. CLC concept consists of transferring oxygen from air to fuel by means of a solid oxygen carrier (OC) which transfers oxygen between two reactors; an air reactor and a fuel reactor, without the need for direct air–fuel contact [13]. This process allows for efficient combustion while inherently capturing CO_2 for sequestration or other applications [13]. Studies have demonstrated that Bio-CLC can achieve lower CO_2 capture costs (£62/tonne) and energy penalties compared to other CO_2 separation

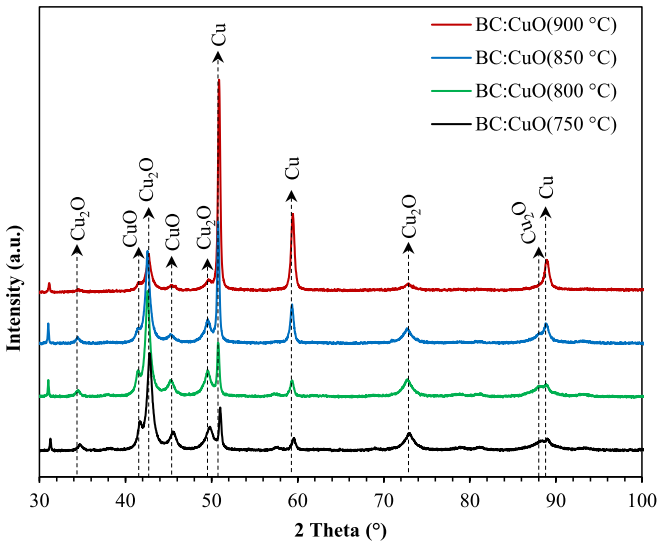

Fig. 6. XRD analysis of CuO (Inoxia) used in the combustion of biochar at 750–900 °C.

technologies including oxyfuel, co-fire, amine scrubbing, and Bio-IGCC [7,11,14], making it a highly economical option for carbon-negative energy production. In these days, chemical looping technologies has been showing commercialisation progress by two industry leaders: Babcock & Wilcox (USA), in partnership with The Ohio State University, through their "Brightloop Chemical Looping" process, and Pure Alchemi (UK) with their "Renewable Combustion" technology. Furthermore, the world's largest CLC demonstration unit is being built close to the city of Chengdu in China with the CHEERS project, which is a collaborative project between Europe and China.

Chemical looping with oxygen uncoupling (CLOU), a variant of CLC, allows oxygen carriers such as CuO, Co_3O_4, and Mn_2O_3 to release gaseous oxygen at elevated temperatures, enabling more efficient combustion of solid fuels like coal, biomass, biochar [15–18]. Various studies have demonstrated the effectiveness of different oxygen carriers in CLC and CLOU using a range of bio-based fuels. Research by Adánez-Rubio et al., [19] demonstrated that CLOU systems achieve faster fuel combustion rates compared to conventional CLC. Skulimowska et al. [20] explored the use of copper-based oxygen carriers (Cu60FA and Cu40FA) with char from Sobieski coal and wood chips at 925 °C, achieving fuel conversion rates of 90 % and 98 %, respectively. Gogolev et al. [21] tested German wood char with ilmenite as oxygen carrier in a 10 kWth CLC pilot fluidised bed reactor, reporting a 94 % conversion rate. In a similar setup, Gogolev et al. [22] investigated straw pellets with a braunite OC in a 60 kWth CLC pilot system, achieving 80 % conversion. Mendiara et al. [11] used olive stones as the fuel with iron ore as the oxygen carrier in a 0.5 kWth pilot system, with a fuel conversion of nearly 99 %. Additionally, Mei et al. [14] reported a 99 % conversion rate using commercial biochar with manganese ore in a 10 kWth fluidised bed reactor. Jiang et al. [23] achieved a 98.5 % conversion using pine sawdust and rice husk with natural hematite in dual circulating fluidised beds at 900 °C.

It has been found that the selection of appropriate metal oxides as oxygen carriers plays a crucial role in determining the combustion efficiency and CO_2 capture. Particularly, CuO-based oxygen carriers have shown significant enhancement in combustion efficiency and CO_2 capture [24]. The effectiveness of CuO-based oxygen carriers in the combustion of hardwood biochar at a temperature range of 750–900 °C, was demonstrated by Kwong et al. [25], while similar results for biochar

Table 3
Combustion efficiency of biochar with CuO under ϕ = 1.0, 1.5, 2.0 at 850 °C.

Stoichiometric Ratio (ϕ)	$V_{CO2,max}$ (mL)	$V_{CO2,measured}$ (mL)	Combustion Efficiency (vol.%)*
1.0	336.1	239.3	71.2 ± 2.7
1.5	336.1	321.7	95.7 ± 8.6
2.0	336.1	325.2	96.8 ± 8.5

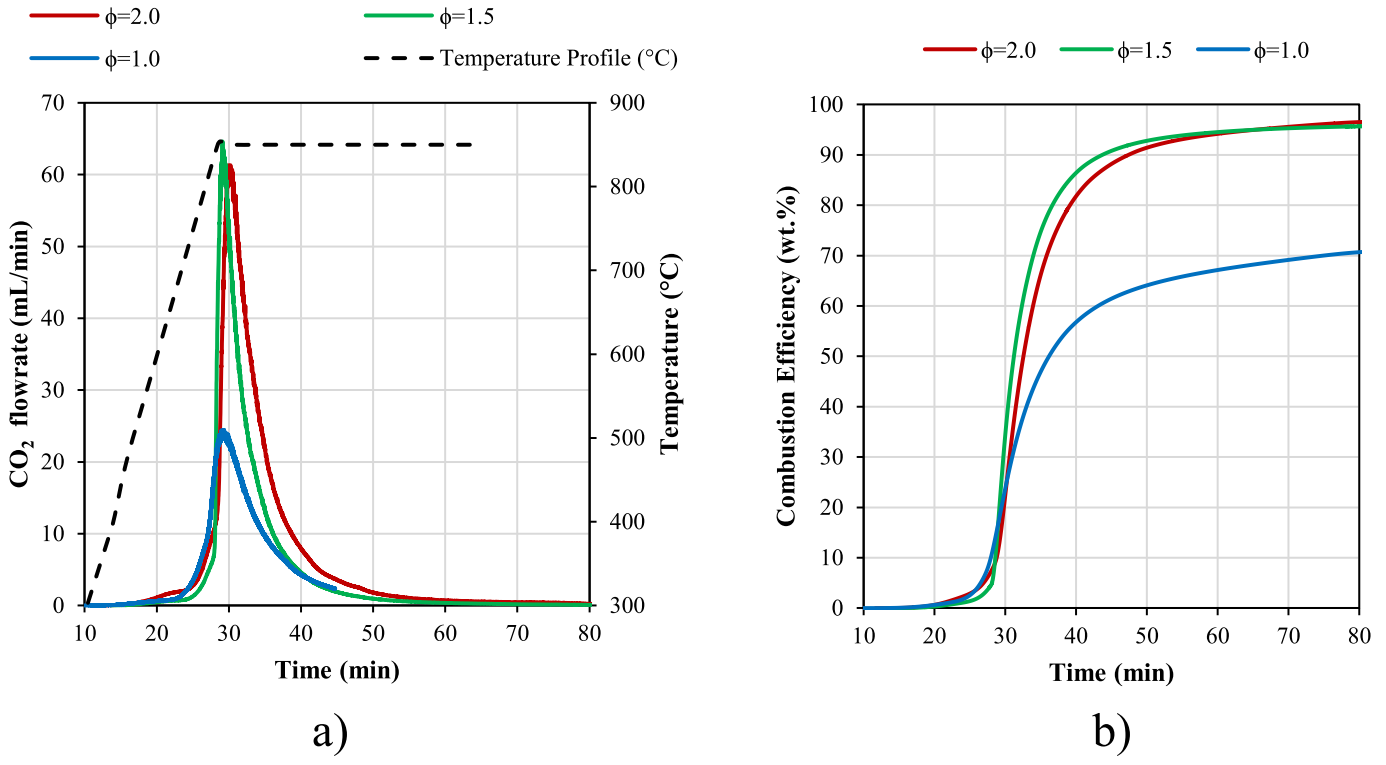

Fig. 7. A) co_2 flow rate and b) Combustion efficiency of the biochar combustion with CuO (Inoxia) at 850 °C with a stoichiometric ratio of ϕ = 1.0, 1.5, and 2.0.

Fig. 8. Visual images of CuO (Inoxia) used in the combustion of biochar at 850 °C under stoichiometric ratio of ϕ = 1.0, 1.5, and 2.0.

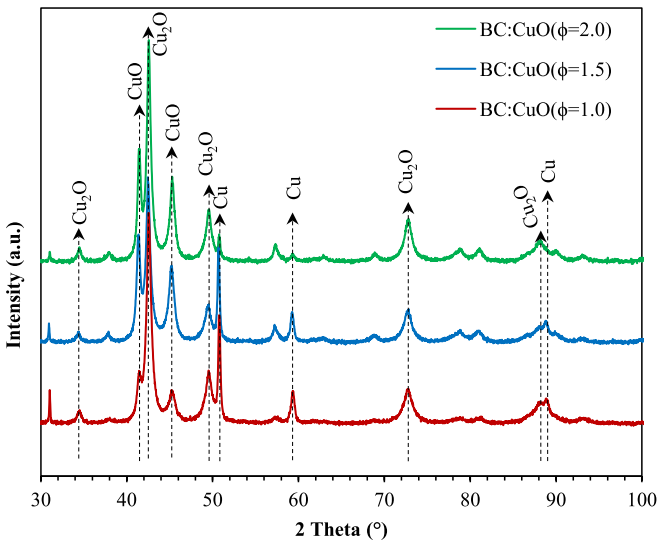

Fig. 9. XRD analysis of CuO (Inoxia) used in the combustion of biochar at 850 °C under the stoichiometric ratio of ϕ = 1.0, 1.5, and 2.0.

combustion with CuO were confirmed by Kuang et al. [26]. In this regard, previous results indicate that the stoichiometric ratio of CuO to char influences the combustion efficiency as a result of a larger volume of oxygen available to be released from CuO. Skulimowska et al. [20] reported efficiencies of a 90 and 97 % using a ratio (CuO to char) of 1.0 and 1.5, respectively.

Although previous studies have demonstrated the effectiveness of CuO-based oxygen carriers in CLC and its oxygen uncoupling variant (CLOU), the impact of CuO's preparation method on the combustion of solid fuels, particularly in biochar, remains underexplored. This study addresses this gap by comparing two commercially sourced CuO materials and two lab-synthesised CuO/Al_2O_3 composites, prepared via co-precipitation and wet impregnation, under identical operational conditions. By evaluating combustion efficiency, redox stability, and oxygen release capacity, this work provides the first systematic assessment of how CuO quality influences biochar combustion performance in a CLOU system. The insights gained are critical for the design of more effective oxygen carriers in CO_2-negative bioenergy applications.

2. Material and methods

2.1. Metal oxide preparation and characterisation

The CuO/Al_2O_3 composite, with a mass ratio of 80:20, was prepared using the coprecipitation method described before [27]. 1.26 M of Cu $(NO_3)_2$ and 0.42 M of $Al(NO_3)_3$ were mixed homogeneously for approximately 5 min. The volumes of each solution were chosen to achieve the desired 80:20 mass ratio of CuO to Al_2O_3 in the final metal oxide composite. Subsequently, 30 vol% of excess sodium carbonate solution (Na_2CO_3, 2.83 M) was slowly added to the mixture to precipitate the metals. This final mixture was stirred using a magnetic stirrer for 15 min. The resulting slurry was centrifuged at 4000 rpm for 10 min. The precipitate, containing excess sodium ions, was washed off using deionised water. The centrifugation and washing process was repeated until the pH of the solution was approximately neutral, indicating that all sodium ions had been removed. After drying in an oven at 110 °C for 12 h, the precipitate was calcined/oxidised in a muffle furnace under static air in a two-stage temperature profile. First, the samples were heated from room temperature to 650 °C with at a rate of 20 °C/min and held for 1 h. The temperature was then increased to 850 °C at the same heating rate and maintained for 3 h. Finally, the samples were gradually cooled to room temperature. The final sample was denoted as "Cu80Al20-CP".

A similar method was employed to produce another CuO/Al_2O_3 sample, using an incipient wet-impregnation technique. In this approach, the aluminium nitrate solution was replaced with aluminium oxide (20 % in H_2O as a colloidal dispersion, supplied by Alfa Aesar). The ratio and process conditions were kept identical to those described in the coprecipitation method above. The resulting sample was designated as "Cu80Al20-WI."

XRD: Crystalline phases prepared CuO samples were measured using a X-ray powder diffractometer (XRD, Siemens D500) using Cu-Kα at 40 kV and 35 mA. Each sample was scanned over a 2θ = 10°–100° with 0.05° as step size and 2 s as step time. Joint Committee on Powder Diffraction Standards (JCPDS) were used to correlate the XRD results.

Surface Imaging: The surface morphology, agglomeration, and sintering of used CuO were determined using aLeica DM4 Fluorescence Microscope and using a HONOR camera. Additionally, the elemental characterisation has been identified by Energy-Dispersive X-ray Spectroscopy (EDS) mapping and spectrums using Oxford X-Max spectroscopy.

2.2. Preparation of biochar and characterisation

The biochars used in this study were produced through pyrolysis in a muffle furnace under an inert atmosphere. Approximately 100 g of Whitewood (WW), derived from sawdust residues in Northern Ireland (UK) and supplied by Wolseley, was placed in a covered porcelain crucible. The crucible was then placed in a muffle furnace and heated from room temperature to 650 °C at a rate of 25 °C/min. Once the target temperature was reached, the sample was held at 650 °C for 30 min, and then the samples were cooled down to room temperature with a heating

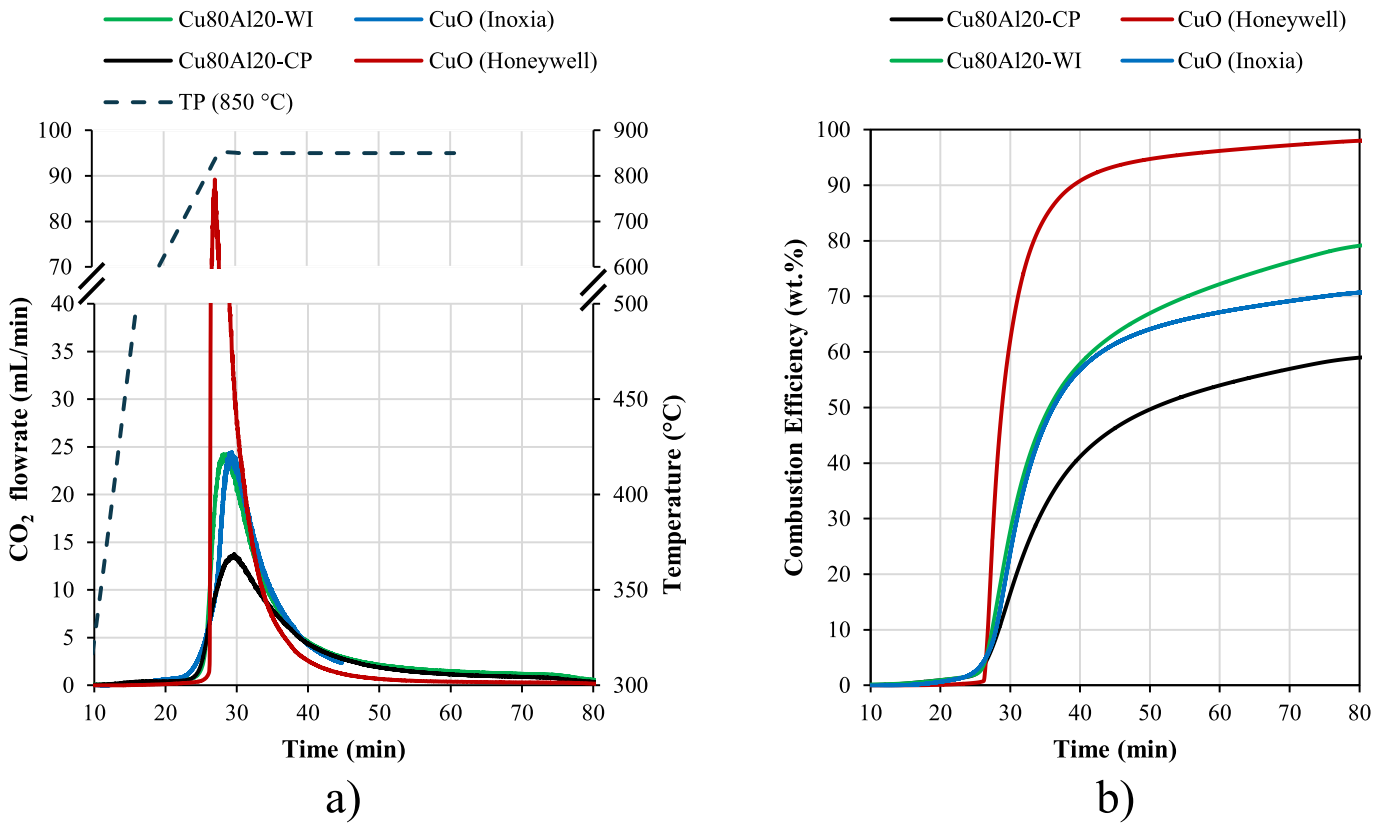

Fig. 10. A) co_2 flow rate and b) Combustion efficiency of the biochar combustion with different CuO sources; CuO (Honeywell), CuO (Inoxia), Cu80Al20-CP, and Cu80Al20-WI at 850 °C under ϕ = 1.0.

Table 4
Effects of CuO source on biochar combustion efficiency at 850°C and ϕ = 1.0.

CuO Source	$V_{CO2,max}$ (mL)	$V_{CO2,measured}$ (mL)	Combustion Efficiency (vol.%)*
CuO-Honeywell	336.1	330.4	98.3 ± 10.2
CuO-Inoxia	336.1	239.3	71.2 ± 2.7
Cu80Al20-WI	336.1	269.2	80.1 ± 3.3
Cu80Al20-CP	336.1	200.0	59.5 ± 3.2

rate of 25 °C/min. Proximate analysis of the prepared biochar was performed in a TA-Q500 using the procedure modified from the previous studies [28,29] to identify the composition of moisture (M), Volatile Matter (VM), Fixed Carbon (FC), and Ash. Furthermore, the elemental compositions (carbon (C), hydrogen (H), nitrogen (N)) of the biomass feedstocks were determined using a LECO CHN 628; oxygen (O) content was calculated by difference [30–33].

2.3. Chemical looping combustion of biochar

Effects of Temperature: The combustion reaction of biochar with Cu-based metal oxides was investigated with a lab-scale fixed-bed reactor unit (Fig. 1). To investigate the effects of temperature on the combustion efficiency of biochar, the following experimental conditions were used: approximately ~0.2 g of biochar was physically mixed with the stoichiometrically required amount of CuO (~2.56 g, supplied from Inoxia with 98.5 % purity) in a porcelain crucible. The stoichiometric ratio (ϕ) used in this study is defined as the molar ratio of oxygen available from the CuO reduction to Cu_2O to the amount of oxygen required for the complete combustion of carbon and hydrogen in the biochar. A ϕ = 1.0 indicates that the amount of CuO provides exactly the stoichiometric oxygen required to oxidise all carbon to CO_2 [6].

The mixture of biochar and CuO were placed in the quartz reactor located in furnace and heated from room temperature to the desired temperature (750, 800, 850 and 900 °C) with a heating rate of 30 °C/

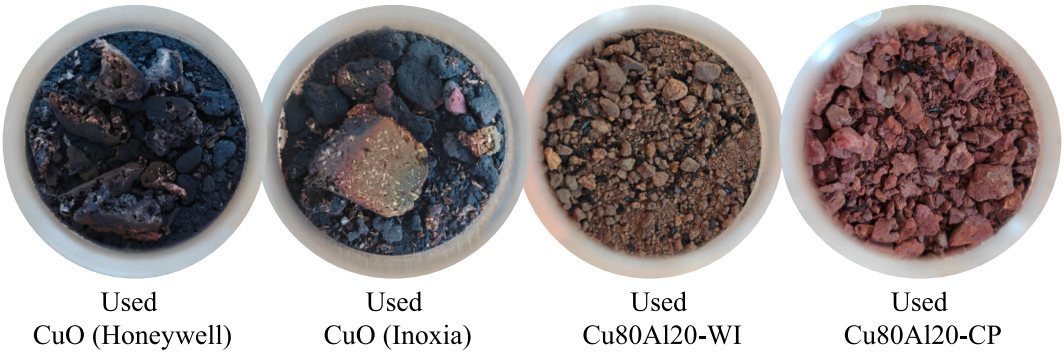

Fig. 11. Visual images of CuO (Honeywell), CuO (Inoxia), Cu80Al20-CP, and Cu80Al20-WI used in the combustion of biochar at 850 °C under ϕ = 1.0.

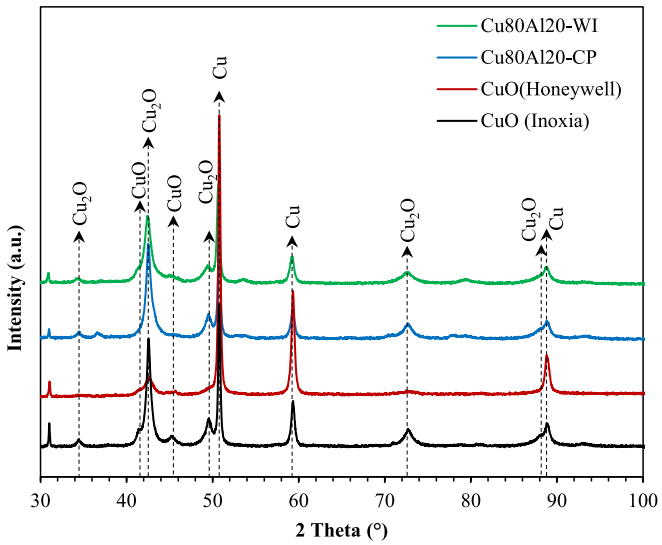

Fig. 12. XRD results of CuO (Honeywell), CuO (Inoxia), Cu80Al20-CP, and Cu80Al20-WI used in the combustion of biochar at 850 °C under ϕ = 1.0.

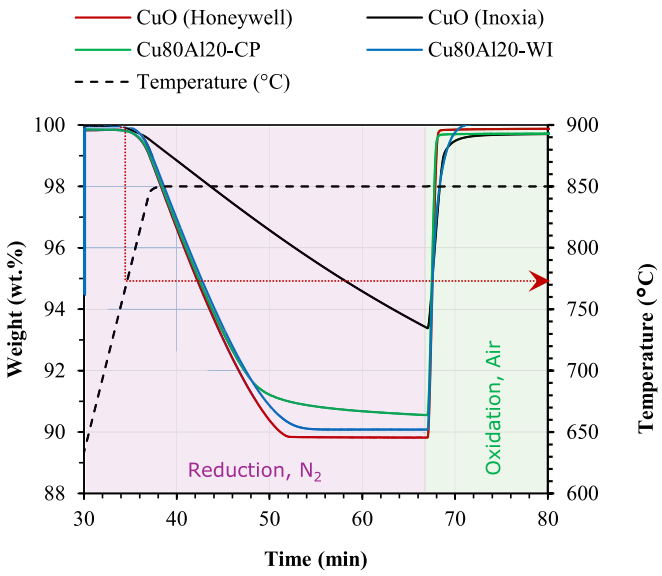

Fig. 13. Single redox (reduction–oxidation) cycle for four different CuO samples; CuO (Honeywell), CuO (Inoxia), Cu80Al20-CP, and Cu80Al20-WI at 850 °C.

min under an inert N_2 stream of 60 mL/min. Once the temperature set point was reached, the temperature remained constant for 45–60 mins. Initially, the gas composition analysis was conducted using a gas chromatograph (GC) equipped with both a flame ionisation detector (FID) and a thermal conductivity detector (TCD). The GC results demonstrated that the gaseous products consisted exclusively of CO_2 and N_2, with no detectable hydrocarbons present in the flue stream. Therefore, throughout the experiment, the concentration of CO_2 in the combustion gases (flue gas) was monitored constantly using an online CO_2 sensor (supplied from Gas Sensing Solutions with a range 0–100 vol%), until complete combustion (or no CO_2 release) had been achieved.

Effects of Stoichiometric Ratio: The effect of the stoichiometric ratio of OC to biochar on combustion efficiency was investigated using different ratios of 1.0, 1.5, and 2.0. For each 0.2 g of biochar requires ~2.56 g of CuO for the stochiometric ratio of 1.0, ~3.84 g of CuO for the stochiometric ratio of 1.5, and ~5.12 g of CuO for the stochiometric ratio of 2.0. The biochar combustion behaviour was investigated using the same experimental produce provided in the previous section "Effects of Temperature" as above at a combustion temperature of 850 °C. The concentration of CO_2 in the combustion gases was monitored constantly using an online sensor.

Effect of CuO Source: The effect of CuO source on combustion behaviour was investigated using two commercially available CuO (supplied from Inoxia and Honeywell) and two CuO/Al_2O_3 samples produced by the co-precipitation and incipient wet-impregnation methods. For each 0.2 g of biochar, ~2.56 g of commercially available CuO requires or ~3.20 g of CuO/Al_2O_3 prepared by co-precipitation and incipient wet-impregnation methods. The differences are due to the active CuO ratio in commercially available CuO (100 wt%) and CuO/Al_2O_3 (80 wt%). The biochar combustion behaviour was investigated using the same experimental procedure at a combustion temperature of 850 °C.

Data Processing: The CO_2 flow was derived from the CO_2 concentration recorded by the in-line CO_2 sensor using the following equation:

$$Q_{CO_2} = \frac{Q_{N_2} * x_{CO_2}}{100 - x_{CO_2}} \quad (1)$$

where, Q_{CO2} and Q_{N2} represent the online flow rates of CO_2 in the flue gas and known N_2 as the carrier gas, respectively (mL/min). X_{CO2} denotes the volumetric concentration of CO_2 measured in the flue gas.

Total CO_2 volume was measured after combustion of biochar with CuO by:

$$V_{CO_2} = \sum_{t_i}^{t_f} \left(Q_{CO_2,t} + Q_{CO_2,t+\Delta t}\right)\Delta t \quad (2)$$

where, V_{CO2} represents the total volume of CO_2 produced through the combustion of biochar. $Q_{CO2,t}$ and $Q_{CO2,t+1}$ (mL/min) represent the online flow rates of CO_2 in the flue gas at t and t + Δt. Δt represents the tie interval between two readings by CO_2 sensor.

The combustion efficiency was then determined by:

$$Combustion\,(vol.\%) = \frac{V_{CO_2,measured}}{V_{CO_2,theoretical}} * 100 \quad (3)$$

where, $V_{CO2,measured}$ (mL) represents the total volume of CO_2 produced through the combustion of biochar and $V_{CO2,theoretical}$ (mL) represents the maximum volume of CO_2 can be produced through the complete combustion of biochar.

Results are presented with error bars that represent the standard deviation of the replicated experiments calculated using Equation (4).

$$s = \sqrt{\frac{1}{(n-1)}\sum_{i=1}^{n}(x_i - \bar{x})^2} \quad (4)$$

where, s is the sample standard deviation, n represents the number of data points in the dataset, x_i represents an individual data point in the dataset, $\bar{x}$ is the average of data set.

2.4. Redox properties of CuO sourced from different suppliers

To assess the variations in the performance of CuO sourced from different suppliers, the CuO samples were evaluated in six continuous reduction–oxidation (redox) cycles. The four types of CuO were individually investigated in this study: two commercially available CuO samples (supplied by Inoxia and Honeywell) and two CuO/Al_2O_3 samples produced via co-precipitation and incipient wet-impregnation. The experiments were conducted with a thermogravimetric analyser (TGA; Q500 – TA Instruments). Approximately 30–50 mg of CuO sample was loaded into a platinum pan with a 10 mm diameter. The sample was first heated from room temperature to 110 °C at a rate of 40 °C/min under a 100 mL/min flow of N_2 and held for 10 min to remove moisture. For the reduction reaction (R1), the sample was then heated to 850 °C at a rate

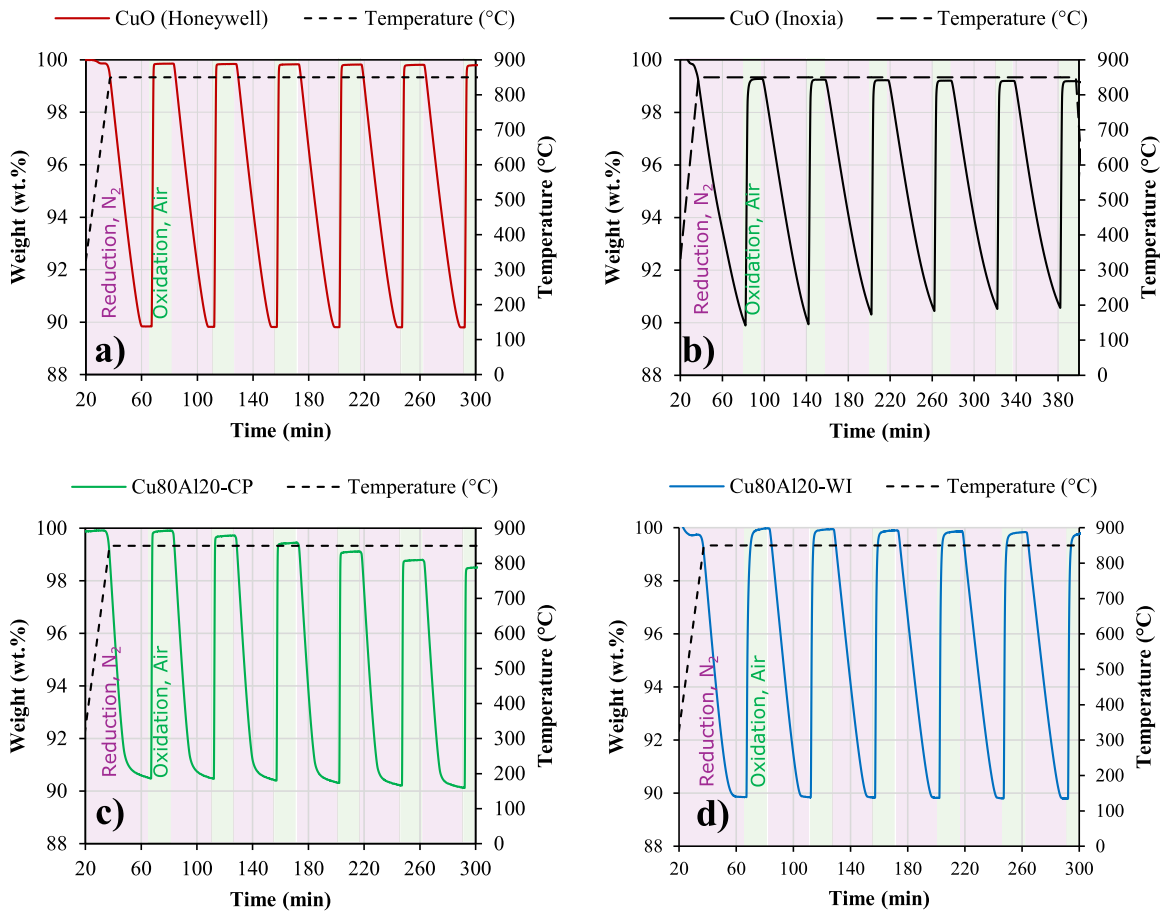

Fig. 14. Six continuous redox (reduction–oxidation) cycles for four different CuO samples; a) CuO (Honeywell), b) CuO (Inoxia), c) Cu80Al20-CP, and d) Cu80Al20-WI at 850 °C (reduction with N_2 and oxidation with air at 850 °C).

of 30 °C/min and held for 30 min under an inert N_2 flow of 100 mL/min. Then, N_2 was replaced with air at the same temperature to observe the oxidation (reverse R1) of the reduced Cu-oxide. The oxidation step was held isothermal for 15 min. The reversible redox reactions for CuO are described by Reaction R1 [34].

$2CuO_{(s)} \rightleftharpoons Cu_2O_{(s)} + ½\ O_{2(g)}$ (R1)

The reduction and oxidation level of CuO supplied from different sources are determined by Equations (5) and (6), respectively [35]

$$x_{red} = \frac{m_{ox} - m}{m_{ox} - m_{red}} \tag{5}$$

$$x_{ox} = 1 - \frac{m_{ox} - m}{m_{ox} - m_{red}} \tag{6}$$

where *m denotes the actual mass of metal oxide at T, m_{ox} denotes its fully oxidised mass, and m_{red} denotes its reduced mass.*

3. Results and discussions

3.1. Characterisation of biochar

The proximate and ultimate analysis results for the raw Whitewood (WW) and the biochar produced from WW at 650 °C are presented in Table 1. The ultimate analysis reveals a significant increase in carbon content (from 46.5 wt% to 90.0 wt%), accompanied by a substantial decrease in hydrogen, nitrogen, and oxygen content after pyrolysis. Additionally, the rise in carbon content is reflected by a proportional increase in fixed carbon (FC) from 12.4 wt% to 81.2 wt% and a decrease in volatile matter (VM) from 80.6 wt% to 11.0 wt%. Throughout the pyrolysis process, the ash content increased only slightly, from 0.4 to 1.1 wt%, indicating that this biochar holds significant potential for CLC due to its relatively low ash content.

3.2. Characterisation of produced CuO

Fig. 2 shows the XRD diffraction patterns of commercially supplied CuO i.e. CuO (Honeywell) and CuO (Inoxia) and synthesised CuO samples i.e. Cu80Al20-CP (prepared by coprecipitation) and Cu80Al20-WI (prepared by wet-impregnation). The XRD patterns confirmed that the successful synthesis of CuO with co-precipitation (Cu80Al20-CP) and wet-impregnation (Cu80Al20-WI) (COD no: 1100028). However, unidentified peaks at roughly 36° and 43° can be attributed to impurities.

3.3. Chemical looping combustion of biochar

Combustion profiles of biochar: Fig. 3 shows the CO_2 flow rate released during the combustion of biochar with CuO at 800 °C and 900 °C. The combustion profile highlights two distinct stages. Stage 1 represents the combustion initiated during non-isothermal heating stage while stage 2 represents the biochar combustion at isothermal conditions, i.e. 800 and 900 °C. The combustion efficiency and the amount of CO_2 released from the combustion of biomass with CuO depends upon the combustion temperature (Fig. 3). The initial CO_2 release occurred at 400 °C (Fig. 3) due to the combustion of volatiles in the biochar, which is consistent with findings by Güleç et al. [17], in which higher hydrocarbons (n-heptane and n-hexadecane) were oxidised by CuO at 360–540 °C. In stage 2, the CuO release its oxygen due to the thermal decomposition thanks to CLOU properties and gas phase oxygen react

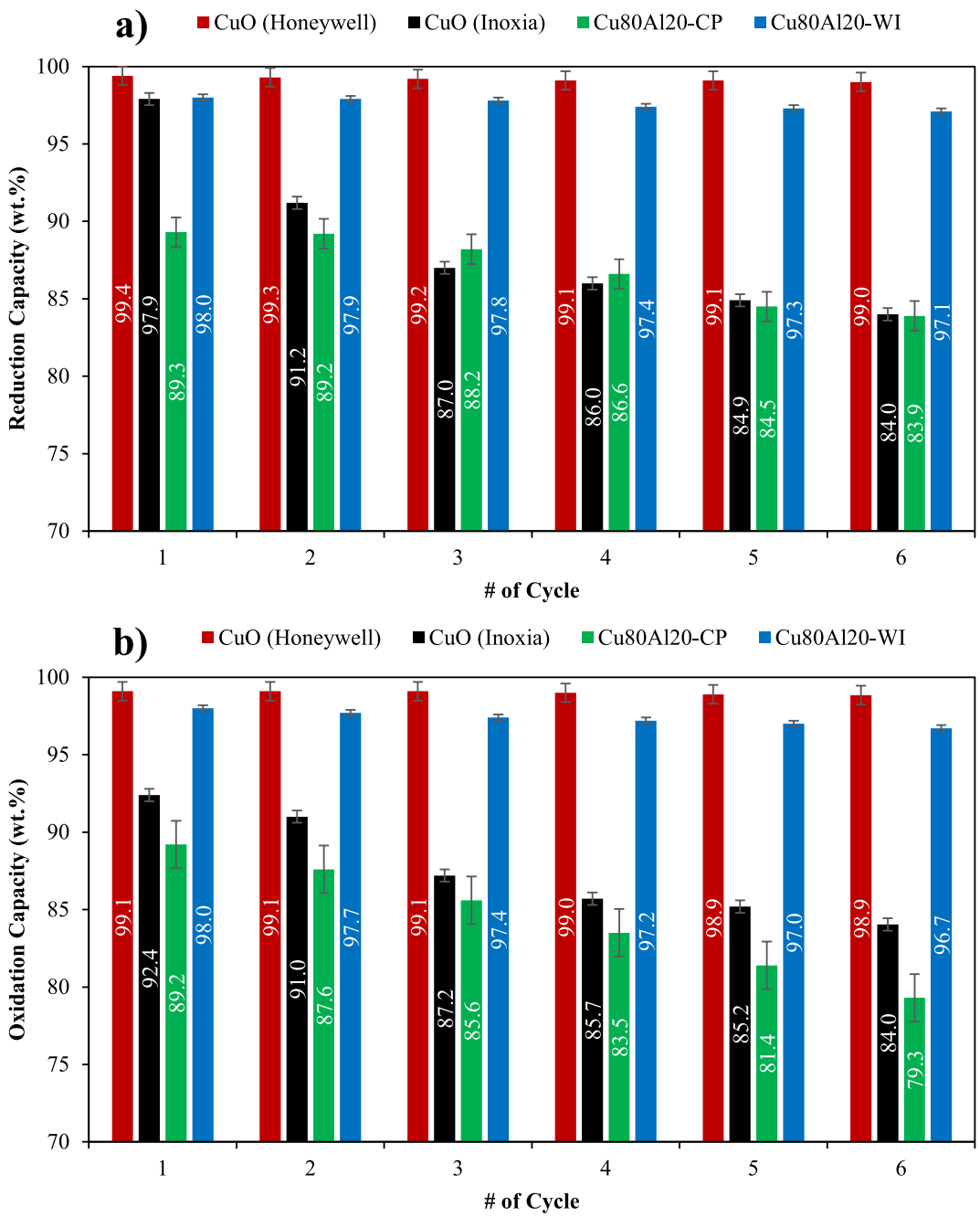

Fig. 15. A) reduction capacity and b) oxidation capacity of cuo (honeywell), cuo (inoxia), cu80al20-cp, and cu80al20-wi at 850 °C. (reduction with N_2 and oxidation with air at 850 °C).

with solid biochar [36].

Effects of Temperature: Table 2 and Fig. 4 demonstrate the combustion efficiency of biochar with CuO at a range of 750 °C to 900 °C. Combustion efficiency was 58.0 ± 4.0 vol% at 750 °C and increased to 98.2 ± 2.4 vol% at 900 °C. The combustion efficiency increases by increasing temperature as a result of a fast oxygen release rate from CuO. As the volume of available gaseous O_2 increases, there is increased availability for the biochar to combust, and therefore release more CO_2, which explains the trend of increasing CO_2 flow rate by temperature (Fig. 4). The temperature dependency is in agreement with previous reports confirming an increase in the combustion efficiency with temperature from 650 °C to 1050 °C [37] and higher temperatures are proposed for the complete combustion of biochar [23,38,39]. The variability in combustion efficiency is attributed to the potential inhomogeneous mixing of biochar and CuO in the crucible, which may have caused non-uniform oxygen transfer and incomplete combustion.

Fig. 5 (and Fig. S1) shows visual images of CuO (Inoxia) used in the combustion of biochar at 750 to 900 °C, and Fig. 6 provides the corresponding XRD analysis of CuO (Inoxia) after combustion within the same temperature range. Fig. 5 demonstrates clear agglomeration of the CuO particles at higher operating temperatures (850–900 °C), with significantly less agglomeration observed at lower temperatures (750–800 °C). The agglomeration at high temperatures could be attributed to a lack of support in the metal oxide structure and the low melting point of Cu. It is visually evident that the agglomerated particles consist of reduced metal oxides and ash components, although some particles exhibit agglomeration of only Cu, Cu_2O, and possible CuO.

The XRD analysis in Fig. 6 confirms the presence of characteristic

peaks for metallic Cu at 50.9°, 59.2°, and 88.9°(COD-9011604), as well as characteristic peaks for Cu_2O at 34.3°, 42.4°, 49.5°, 72.5°, and 88.0° (COD-9005769). These peaks were observed following the CLC of biochar with CuO at temperatures between 750–900 °C. It is likely that CuO reduces directly to Cu [17] during the combustion of volatiles, bypassing the sequential reduction steps CuO → Cu_4O_3 → Cu_2O → Cu. At higher temperatures, remaining CuO releases oxygen to oxidise the biochar, resulting in its reduction to Cu_2O [15–18]. Consequently, the final, used CuO sample consists of a mixture of Cu and Cu_2O. Since CuO reduces only to Cu_2O under thermal decomposition due to its CLOU properties [15–18]. Any further reduction to metallic Cu is likely due to interactions between gas-phase volatiles and solid-phase CuO at low temperatures. Similar reductions have been observed in the CLC of n-hexadecane with CuO, where further reduction to Cu was attributed to limited external mass transfer at low combustion temperatures [17]. Chuang et al. [27] reported that the reduction of CuO by CO or H_2 follows a shrinking-core mechanism, progressing through an intermediate Cu_2O phase at higher temperatures when external mass transfer controls the reaction rate. However, at lower temperatures, with minimal external mass transfer, CuO can reduce directly to metallic Cu.

Effects of Stoichiometric Ratio: Fig. 7 and Table 3 show the combustion efficiency of biochar with CuO at stoichiometric ratios of ϕ = 1.0, 1.5, and 2.0 at 850 °C. Both illustrate a consistent trend of increasing combustion efficiency with higher stoichiometric ratios. At ϕ = 1.0, combustion efficiency was 71.2 vol%, increased to 95.7 vol% at ϕ = 1.5. A further increase was observed as 96.8 vol% at ϕ = 2.0. The improvement in combustion efficiency with higher stoichiometric ratios is due to the increased availability of oxygen for biochar combustion. However, beyond ϕ = 1.5, further increases in oxygen supply have a diminishing combustion efficiency, as the reaction becomes limited by the carbon content in the biochar. Investigating the stochiometric ratio between ϕ = 1.0–1.5, which has not been investigated in this study, is important to optimise the stochiometric ratio with maximum combustion efficiency. This trend is consistent with the TGA analysis reported before [20], which showed 90 vol% efficiency at ϕ = 1.0 and 97 vol% at ϕ = 1.5. Similarly, Adánez et al. [40] achieved less than 99 vol% conversion at ϕ = 1.4 using a 10-kW prototype system.

Fig. 8 (and Fig. S2) shows visual images of used CuO (Inoxia) under ϕ = 1.0, 1.5, 2.0 at 850 °C, and Fig. 9 provides the corresponding XRD analysis of used CuO (Inoxia). Regardless of the stochiometric ratio used, CuO (Inoxia) shows a significant agglomeration at 850 °C.

The XRD analysis presented in Fig. 9 confirms the presence of characteristic peaks for metallic Cu at 50.9°, 59.2°, and 88.9°(COD-9011604), after testing CuO under a stoichiometric ratio of ϕ = 1.0 at 850 °C. As the stoichiometric ratio increases to ϕ = 1.5 and 2.0, the intensity of the characteristic Cu peaks decreases, while the peaks corresponding to Cu_2O at 34.3°, 42.4°, 49.5°, 72.5°, and 88.0°(COD-9005769) and CuO at 41.5°, 45.2°, 45.5°, 57.1°, 72.6°, and 81.0° (COD-9016057) become more prominent. This shift is likely due to the thermal decomposition of excess CuO to Cu_2O at 850 °C.

Effect of CuO Source: Fig. 10 and Table 4 present the combustion efficiency of biochar using four different CuO samples; two commercial (supplied from Inoxia and Honeywell) and two lab-prepared (Cu80Al20-CP and Cu80Al20-WI). A significant variation is observed between the commercial samples: CuO (Honeywell) achieves a combustion efficiency of 98.3 vol%, while CuO (Inoxia) only reaches 71.2 vol% at a stoichiometric ratio of 1.0 and 850 °C. Similarly, the lab-prepared samples show differing combustion efficiencies, with Cu80Al20-WI at 80.1 vol% and Cu80Al20-CP at 59.5 vol%. The combustion efficiency of metal oxides is influenced by factors such as surface area, which determines the availability of active sites for oxygen in reduction/oxidation CLC processes. High-quality CuO samples, characterised by larger surface areas, provide greater oxygen availability for carbon oxidation, thereby improving combustion efficiency and increasing CO_2 release. These results align with previous studies [24,27], which report that high-quality CuO samples exhibit reduced agglomeration, maintain surface area, and consequently deliver superior combustion performance.

Fig. 11 (and Fig. S3) shows visual images of used CuO (Honeywell), CuO (Inoxia), Cu80Al20-CP, and Cu80Al20-WI at 850 °C under ϕ = 1.0, and Fig. 12 provides the corresponding XRD analysis of these used Cu-based oxygen carriers. Although the lab-prepared samples (Cu80Al20-CP and Cu80Al20-WI) exhibit some degree of agglomeration, this was consistent with the level of agglomeration observed in their fresh state. Importantly, unlike the commercial samples, the lab-prepared samples did not form large chunks or bulk agglomerates.

The XRD analysis presented in Fig. 12 confirms that all the used CuO samples consists of the characteristic peaks of Cu at 50.9°, 59.2°, and 88.9°(COD-9011604) and Cu_2O at 34.3°, 42.4°, 49.5°, 72.5°, and 88.0° (COD-9005769). The used CuO (Honeywell) showed the highest intensity, which usually points to a combination of high crystallinity, large crystallite size, and high phase concentration of CuO.

3.4. Multiple redox cycles of Cu-based oxygen carriers

Fig. 13 shows that the thermal decomposition of CuO to Cu_2O begins at approximately 770 °C. Although the reaction between CuO and C can be favourable between 200–1000 °C [41] CuO decomposition is not thermodynamically favourable below 700 °C according to the Positive Gibbs free energy values. The oxygen release from the decomposition of CuO to Cu_2O are able to noticeable at around 750 °C [42] and 790 °C [43]. This variation between 700 and 790 °C is due to the decomposition rate of CuO. Since the partial pressure of O_2 released from CuO increases with temperature increasing; while it is lower than 10^{-3} at 750 °C, it is around 15×10^{-3} at 900 °C [16,18,42]. Mattisson et al. [44] also showed that increasing the reaction temperature increases the partial pressure of oxygen released from the decomposition of CuO to Cu_2O, which promotes the rate of oxygen release in CLOU, as demonstrated in Fig. S4 and Fig. S5 (in Supplementary).

Although CuO is one of the most promising oxygen carriers for solid fuel combustion [45] due to its chemical looping with oxygen uncoupling (CLOU) properties, the performance of CuO can vary significantly depending on its preparation method and physicochemical characteristics, such as surface area, particle size, and choice of support material. The decomposition rate of CuO (Inoxia) is notably slower compared to both the other commercial CuO (Honeywell) and the lab-prepared samples (Cu80Al20-CP and Cu80Al20-WI). CuO (Honeywell) achieved the highest reduction capacity, reaching 10.1 wt% at 850 °C within 18 min. The lab-prepared samples (Cu80Al20-WI and Cu80Al20-CP) exhibited similar decomposition profiles, with reductions ranging from 9.3 to 9.9 wt%, slightly below the theoretical maximum of 10.1 wt%. In contrast, CuO (Inoxia) displayed a much lower oxygen release rate of 6.5 wt% over 35 min at 850 °C.

Although both are commercially supplied, CuO (Inoxia) has a particle size of 54 μm which is larger than CuO-Honeywell (10 μm), a physical property which is known to affect the reactivity of OCs Since the reactivity of OCs increases with decreasing particle sizes from micro- to nano-scales [46]. As for the lab-prepared samples, the performance of Cu80Al20-WI and Cu80Al20-CP were attributed to the gas diffusional effect and mass transfer limitations at 850 °C. Chuang et al.[27] studied the oxidation kinetics of CuO/Al_2O_3 prepared by co-precipitation with a Cu loading of 82.5 wt% and proposed that due to Cu atoms having different mobilities in Cu_2O and CuO, the gas's diffusion through the pores of the particles was slower than that of the chemical process and the reaction followed the shrinking core mechanism [27]. The oxygen carrier behaviour of CuO/Al_2O_3 prepared by incipient wet impregnation also provided similar results [47] and discovered stable operation for about 30 h was only attainable at temperatures less than 800 °C in the FR and at 900 °C in the AR [47]. Regardless of reduction rates, the oxidation rates of these four CuO samples were relatively fast (Fig. 13). The instantaneous oxygen carrier reduction and oxidation conversions, which is useful to assess the reduction and oxidation rates and kinetics, are provided in Fig. S5 and Fig. S6 in Supplementary. The faster

decomposition and higher oxygen-carrying capacity are crucial for minimising the residence time of oxygen carriers in fuel and air reactors, allowing for higher cycle frequencies and reducing the required reactor capacity [45].

Figs. 14 and 15 illustrate the six consecutive redox cycles and the reduction/oxidation percentages relative to the theoretical oxygen release and uptake capacities of the four CuO samples. Although six redox cycles are insufficient to fully evaluate the long-term stability of oxygen carriers, this test was intended as a preliminary screening to distinguish materials with potential for further development.

Fig. 14a and 14d demonstrate the stability of CuO (Honeywell) and Cu80Al20-WI after six consecutive reduction and oxidation cycles at 850 °C, with minimal loss in oxygen carrier capacity. CuO (Honeywell) released 99.4 wt% of its theoretical oxygen capacity, which only decreased slightly to 99.0 wt% after six cycles (Fig. 15a), with a similarly stable oxidation profile (Fig. 15b). Likewise, the lab-prepared Cu80Al20-WI showed high stability, releasing 98 wt% of its theoretical oxygen capacity initially, which dropped marginally to 97.1 wt% after six cycles (Fig. 15a), with comparable oxidation stability (Fig. 15b).

Fig. 14b shows that the reduction of CuO (Inoxia) remains below its stoichiometric oxygen release capacity, even when the reduction time is extended to 45 min. In the first cycle, CuO (Inoxia) released 97.8 wt% of its theoretical oxygen capacity, with an oxidation level of 92.4 wt%, but these values dropped significantly to 84 wt% for both reduction and oxidation after six cycles (Fig. 15a and 15b). Although not shown in this manuscript, CuO (Inoxia) experienced significant agglomeration after the first cycle, contributing to the sharp decline in capacity. While the capacity reduction of CuO (Inoxia) was less severe after the second cycle, it remained higher compared to the other CuO samples. The lab-prepared Cu80Al20-CP exhibited a relatively low oxygen release capacity of 89.3 wt% in the first cycle, which gradually declined due to poor oxidation levels, reaching 83.9 wt% after six cycles (Fig. 15b).

4. Conclusions

This study highlights the critical influence of both process conditions and oxygen carrier quality on optimising the CLC of biochar with CuO. Results showed that combustion efficiency significantly increased with temperature, reaching 98.2 vol% at 900 °C, compared to 67.9 vol% at 750 °C. Similarly, increasing the stoichiometric ratio from 1.0 to 1.5 led to an improvement in efficiency from 71.2 vol% to 95.7 vol%. Among the tested oxygen carriers, CuO (Honeywell) exhibited the highest efficiency (98.3 vol%), significantly outperforming CuO (Inoxia) and both lab-prepared variants. Notably, the lab-synthesised Cu80Al20-WI showed better combustion performance (80.1 vol%) and redox stability compared to Cu80Al20-CP (59.5 vol%) at 850 °C. Over multiple redox cycles, CuO (Honeywell) maintained 99.0 wt% of its redox capacity after six cycles, while Cu80Al20-WI retained 97.1 wt%, indicating high thermal stability. In contrast, CuO (Inoxia) and Cu80Al20-CP exhibited degradation, with their capacities decreasing to 84 wt% and 83.9 wt%, respectively, due to agglomeration. These findings underline the necessity of optimising both operational parameters and oxygen carrier synthesis methods to achieve high efficiency and stability in CLC processes. Future work should focus on evaluating long-term redox performance over extended cycles (>100) to assess durability under realistic operating conditions. Additionally, testing in fluidised or circulating fluidised bed reactors, alongside investigation of ash–carrier interactions, attrition resistance, and scale-up potential, will be essential to support the deployment of CLC in BECCS and other CO_2-negative energy systems.

CRediT authorship contribution statement

Fatih Güleç: Writing – review & editing, Writing – original draft, Visualization, Validation, Supervision, Resources, Project administration, Methodology, Investigation, Funding acquisition, Formal analysis, Data curation, Conceptualization. **Ciaran Moyles:** Writing – original draft, Visualization, Methodology, Investigation, Formal analysis, Data curation, Conceptualization. **Harrison Tagg:** Writing – original draft, Visualization, Methodology, Investigation, Formal analysis, Data curation, Conceptualization. **Alexander Marshall:** Writing – original draft, Visualization, Methodology, Investigation, Formal analysis, Data curation, Conceptualization. **Jack Craft:** Writing – original draft, Visualization, Methodology, Investigation, Formal analysis, Data curation, Conceptualization. **Andrew Batchelor:** Writing – original draft, Visualization, Resources, Methodology, Investigation, Formal analysis, Data curation, Conceptualization. **Gabriela Duran-Jimenez:** Writing – original draft, Visualization, Validation, Supervision, Resources, Project administration, Methodology, Investigation, Funding acquisition, Formal analysis, Data curation, Conceptualization.

Declaration of competing interest

The authors declare that they have no known competing financial interests or personal relationships that could have appeared to influence the work reported in this paper.

Acknowledgements

The authors acknowledge the financial support from the University of Nottingham's FPVC Research Acceleration Fund (Dr Fatih Gulec). The authors also gratefully acknowledge the Department of Chemical and Environmental Engineering's support in the research activities of MEng students (Ciaran Moyles, Harrison Tagg, Alexander Marshall, and Jack Craft). This research was partially funded by EPSRC [EP/S036113/1], Connected Everything II.

Appendix A. Supplementary data

Supplementary data to this article can be found online at https://doi.org/10.1016/j.fuel.2025.135685.

Data availability

Data will be made available on request.

References

[1] COP27: Key outcomes and next steps for the UK December 2022; 2022.
[2] A. Åberg, A. Froggatt, R. Peters, Raising climate ambition at COP26; n.d.
[3] World Energy Outlook 2022, n.d. www.iea.org/t&c/.
[4] United Nations Framework Convention on Climate Change, UNFCCC (United Nations Framework Convention on Climate Change), 2023. NDC Synthesis Report 2023. Available at: https://unfccc.int/ndc-synthesis-report-2023, Https://Unfccc.Int/Ndc-Synthesis-Report-2023; 2023.
[5] Net Zero Strategy: Build Back Greener; 2021.
[6] Güleç F, Okolie JA. Decarbonising bioenergy through biomass utilisation in chemical looping combustion and gasification: a review. Environ Chem Lett 2024; 22:121–47. https://doi.org/10.1007/s10311-023-01656-5.
[7] Bhave A, Taylor RHS, Fennell P, Livingston WR, Shah N, Mac Dowell N, et al. Screening and techno-economic assessment of biomass-based power generation with CCS technologies to meet 2050 CO2 targets. Appl Energy 2017;190:481–9. https://doi.org/10.1016/j.apenergy.2016.12.120.
[8] UK Government DESNZ, Biomass Strategy 2023; 2023. www.gov.uk/official-documents.
[9] Mac Dowell N, Fajardy M. Inefficient power generation as an optimal route to negative emissions via BECCS? Environ Res Lett 2017;12. https://doi.org/10.1088/1748-9326/aa67a5.
[10] Booth A, Wentworth J, Biomass for UK energy; 2023.
[11] Mendiara T, Pérez-Astray A, Izquierdo MT, Abad A, de Diego LF, García-Labiano F, et al. Chemical Looping Combustion of different types of biomass in a 0.5 kWth unit. Fuel 2018;211:868–75. https://doi.org/10.1016/j.fuel.2017.09.113.
[12] Shen T, Shen L, Song T. Multiscale gas–solid reaction dynamics of hematite oxygen carrier in chemical looping combustion from fluidized bed thermogravimetric analysis. Energy Fuel 2024;38(10):8909–27.

[13] Ma J, Zhao H, Tian X, Wei Y, Rajendran S, Zhang Y, et al. Chemical looping combustion of coal in a 5 kWth interconnected fluidized bed reactor using hematite as oxygen carrier. Appl Energy 2015;157:304–13.
[14] Mei D, Soleimanisalim AH, Linderholm C, Lyngfelt A, Mattisson T. Reactivity and lifetime assessment of an oxygen releasable manganese ore with biomass fuels in a 10 kWth pilot rig for chemical looping combustion. Fuel Process Technol 2021; 215. https://doi.org/10.1016/j.fuproc.2021.106743.
[15] Imtiaz Q, Hosseini D, Müller CR. Review of oxygen carriers for chemical looping with oxygen uncoupling (CLOU): thermodynamics, material development, and synthesis. Energ Technol 2013;1:633–47. https://doi.org/10.1002/ente.201300099.
[16] Güleç F, Meredith W, Sun CG, Snape CE. Demonstrating the applicability of chemical looping combustion for the regeneration of fluid catalytic cracking catalysts. Chem Eng J 2020;389. https://doi.org/10.1016/j.cej.2020.124492.
[17] Güleç F, Meredith W, Sun CG, Snape CE. Selective low temperature chemical looping combustion of higher alkanes with Cu- and Mn- oxides. Energy 2019;173: 658–66. https://doi.org/10.1016/j.energy.2019.02.099.
[18] Güleç F, Meredith W, Sun CG, Snape CE. A novel approach to CO2 capture in Fluid Catalytic Cracking—Chemical Looping Combustion. Fuel 2019;244:140–50. https://doi.org/10.1016/j.fuel.2019.01.168.
[19] Adánez-Rubio I, Abad A, Gayán P, De Diego LF, García-Labiano F, Adánez J. Identification of operational regions in the Chemical-Looping with Oxygen Uncoupling (CLOU) process with a Cu-based oxygen carrier. Fuel 2012;102: 634–45. https://doi.org/10.1016/j.fuel.2012.06.063.
[20] Skulimowska A, Di Felice L, Kamińska-Pietrzak N, Celińska A, Pławecka M, Hercog J, et al. Chemical looping with oxygen uncoupling (CLOU) and chemical looping combustion (CLC) using copper-enriched oxygen carriers supported on fly ash. Fuel Process Technol 2017;168:123–30. https://doi.org/10.1016/j.fuproc.2017.08.035.
[21] Gogolev I, Soleimanisalim AH, Linderholm C, Lyngfelt A. Commissioning, performance benchmarking, and investigation of alkali emissions in a 10 kWth solid fuel chemical looping combustion pilot. Fuel 2021;287. https://doi.org/10.1016/j.fuel.2020.119530.
[22] Gogolev I, Pikkarainen T, Kauppinen J, Hurskainen M, Lyngfelt A. Alkali emissions characterization in chemical looping combustion of wood, wood char, and straw fuels. Fuel Process Technol 2022;237. https://doi.org/10.1016/j.fuproc.2022.107447.
[23] Jiang S, Shen L, Yan J, Ge H, Song T. Performance in coupled fluidized beds for chemical looping combustion of CO and biomass using hematite as an oxygen carrier. Energy Fuel 2018;32:12721–9. https://doi.org/10.1021/acs.energyfuels.8b02861.
[24] Jin B, Fan Y, Lv Y, Li G, Zhao H, Liang Z. Low concentration Ni doping to intensify redox kinetics of iron-based oxygen carriers for efficient chemical looping reverse water gas shift. Sep Purif Technol 2025;360:131237.
[25] Kwong KY, Harrison ARP, Gebers JC, Dennis JS, Marek EJ. Chemical looping combustion of a biomass char in Fe2O3-, CuO-, and SrFeO3-δ-based oxygen carriers. Energy Fuel 2022;36:9437–49. https://doi.org/10.1021/acs.energyfuels.2c01269.
[26] Kuang C, Wang S, Luo M, Cai J, Zhao J. Investigation of CuO-based oxygen carriers modified by three different ores in chemical looping combustion with solid fuels, Renew. Energy 2020;154:937–48. https://doi.org/10.1016/j.renene.2020.03.027.
[27] Chuang SY, Dennis JS, Hayhurst AN, Scott SA. Kinetics of the chemical looping oxidation of CO by a co-precipitated mixture of CuO and Al2O3, Proc Comb Instit 32 II (2009) 2633–2640. https://doi.org/10.1016/j.proci.2008.06.112.
[28] Duran-Jimenez G, Rodriguez J, Stevens L, Altarawneh S, Batchelor A, Jiang L, et al. Single-step preparation of activated carbons from pine wood, olive stones and nutshells by KOH and microwaves: influence of ultra-microporous for high CO2 capture. Chem Eng J 2024;499. https://doi.org/10.1016/j.cej.2024.156135.
[29] Kostas ET, Williams OSA, Duran-Jimenez G, Tapper AJ, Cooper M, Meehan R, et al. Microwave pyrolysis of Laminaria digitata to produce unique seaweed-derived bio-oils. Biomass Bioenergy 2019;125:41–9. https://doi.org/10.1016/j.biombioe.2019.04.006.
[30] Güleç F, Williams O, Kostas ET, Samson A, Lester E. A comprehensive comparative study on the energy application of chars produced from different biomass feedstocks via hydrothermal conversion, pyrolysis, and torrefaction. Energy Convers Manag 2022;270. https://doi.org/10.1016/j.enconman.2022.116260.
[31] Güleç F, Samson A, Williams O, Kostas ET, Lester E. Biofuel characteristics of chars produced from rapeseed, whitewood, and seaweed via thermal conversion technologies – Impacts of feedstocks and process conditions. Fuel Process Technol 2022;238. https://doi.org/10.1016/j.fuproc.2022.107492.
[32] Durán-Jiménez G, Rodriguez J, Stevens L, Kostas ET, Dodds C. Microwave pyrolysis of waste biomass and synthesis of micro-mesoporous activated carbons: The role of textural properties for CO2 and textile dye adsorption. Chem Eng J 2024;488. https://doi.org/10.1016/j.cej.2024.150926.
[33] Silos-Llamas AK, Sudibyo H, Hernández-Montoya V, Meredith W, Durán-Jiménez G. Fast pyrolysis of agricultural residues: reaction mechanisms and effects of feedstock properties and microwave operating conditions on the yield and product composition. J Anal Appl Pyrolysis 2023;175. https://doi.org/10.1016/j.jaap.2023.106217.
[34] Aghabararnejad M, Patience GS, Chaouki J. TGA and kinetic modelling of Co, Mn and Cu oxides for Chemical Looping Gasification (CLG). Can J Chem Eng 2014;92: 1903–10. https://doi.org/10.1002/cjce.22046.
[35] Cho P, Mattisson T, Lyngfelt A. Defluidization conditions for a fluidized bed of iron oxide-, nickel oxide-, and manganese oxide-containing oxygen carriers for chemical-looping combustion. Ind Eng Chem Res 2006;45:968–77. https://doi.org/10.1021/ie050484d.
[36] Sahir AH, Dansie JK, Cadore AL, Lighty JAS. A comparative process study of chemical-looping combustion (CLC) and chemical-looping with oxygen uncoupling (CLOU) for solid fuels. Int J Greenhouse Gas Control 2014;22:237–43. https://doi.org/10.1016/j.ijggc.2014.01.008.
[37] Sheth MM, Sigdel S, Harichandan AB, Bhoraniya R. Performance of fuel reactor in Chemical Looping Combustion system with various metal oxide particle size and operating temperature. Int J Thermofluids 2023;17. https://doi.org/10.1016/j.ijft.2023.100295.
[38] Chen H, Li Z, Wang R. Design theory of a CLC air reactor with oxygen carrier recirculation and its application to a 3 MWthPilot. Energy Fuel 2021;35:1580–93. https://doi.org/10.1021/acs.energyfuels.0c03111.
[39] Abad A, Adánez J, Gayán P, de Diego LF, García-Labiano F, Sprachmann G. Conceptual design of a 100 MWthCLC unit for solid fuel combustion. Appl Energy 2015;157:462–74. https://doi.org/10.1016/j.apenergy.2015.04.043.
[40] Adánez J, Gayán P, Celaya J, De Diego LF, García-Labiano F, Abad A. Chemical looping combustion in a 10 kWth prototype using a CuO/Al2O3 oxygen carrier: Effect of operating conditions on methane combustion. Ind Eng Chem Res 2006;45: 6075–80. https://doi.org/10.1021/ie060364l.
[41] Siriwardane R, Tian H, Miller D, Richards G, Simonyi T, Poston J. Evaluation of reaction mechanism of coal-metal oxide interactions in chemical-looping combustion. Combust Flame 2010;157:2198–208. https://doi.org/10.1016/j.combustflame.2010.06.008.
[42] Mattisson T, Lyngfelt A, Leion H. Chemical-looping with oxygen uncoupling for combustion of solid fuels. Int J Greenhouse Gas Control 2009;3:11–9. https://doi.org/10.1016/j.ijggc.2008.06.002.
[43] Shabani A, Rahman M, Pudasainee D, Samanta A, Sarkar P, Gupta R. Evaluation of ash-free coal for chemical looping combustion - part I: Thermogravimetric single cycle study and the reaction mechanism. Can J Chem Eng 2017;95:623–33. https://doi.org/10.1002/cjce.22721.
[44] Mattisson T. Materials for chemical-looping with oxygen uncoupling. ISRN Chem Eng 2013;2013:1–19. https://doi.org/10.1155/2013/526375.
[45] Güleç F. Kinetic analysis of solid fuel combustion in chemical looping for clean energy conversion. Fuel 2024;378. https://doi.org/10.1016/j.fuel.2024.132911.
[46] Akram W, Sanjay, Hassan MA. Chemical looping combustion with nanosize oxygen carrier: a review. Int J Environ Sci Technol 2021;18:787–98. https://doi.org/10.1007/s13762-020-02840-8.
[47] Rosa Forero C, Forero CR. High temperature behaviour of CuO-based oxygen carriers for chemical-looping combustion process Comportamiento a alta temperatura de transportadores sólidos de oxígeno de base cobre para el proceso “chemical looping combustion” High temperature behaviour of CuO-based oxygen carriers for chemical-looping combustion process; 2014. https://www.researchgate.net/publication/317500343.